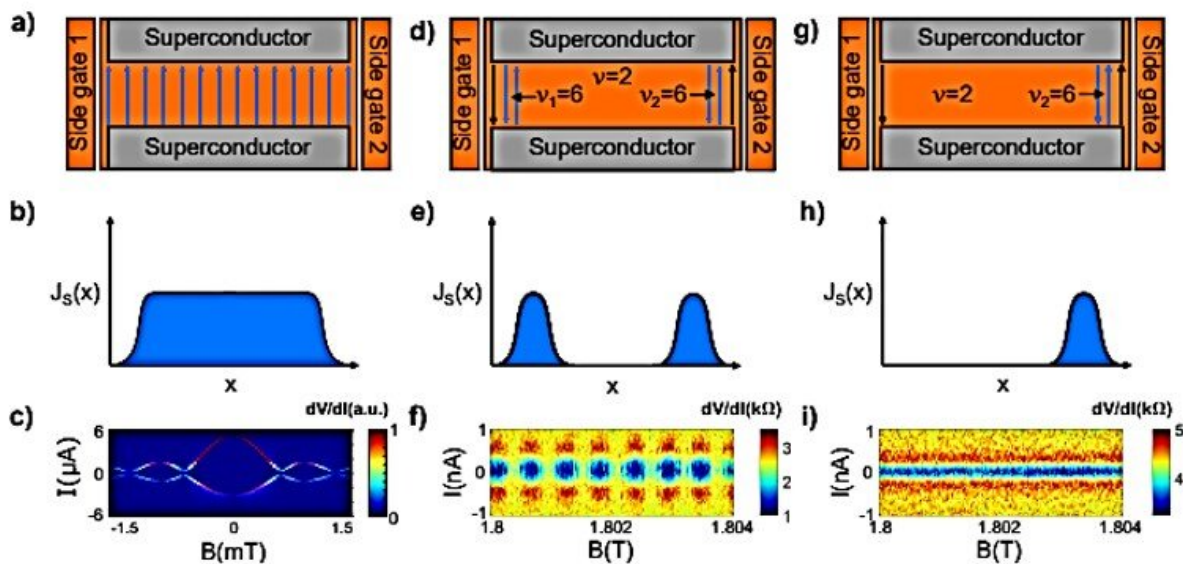# Quantum Hall-based superconducting interference device

September 24 2019, by Thamarasee Jeewandara

Three column comparison of the supercurrent distributions and the resulting magnetic interference patterns. a) Diagram of supercurrent flow at low magnetic fields, resulting in a uniform distribution shown in panel (b). c) Measurement of the second device at low magnetic field showing a typical Fraunhofer interference pattern with period of ~ 0.7 mT, which indicates a uniform supercurrent distribution. Data is a numerical derivative of the measured I-V curves (arbitrary units). T= 230 mK. d) Schematic of QH edges when both side gates are applied (bulk $\nu = 2$, locally induced $\nu = 6$ on each edge). The closely spaced counterpropagating states support supercurrents on both edges of the sample, resulting in the distribution shown in panel (e). Panel (f) shows the SQUID (superconducting quantum interference device)-like magnetic interference pattern of quantum Hall supercurrent corresponding to panel (d)
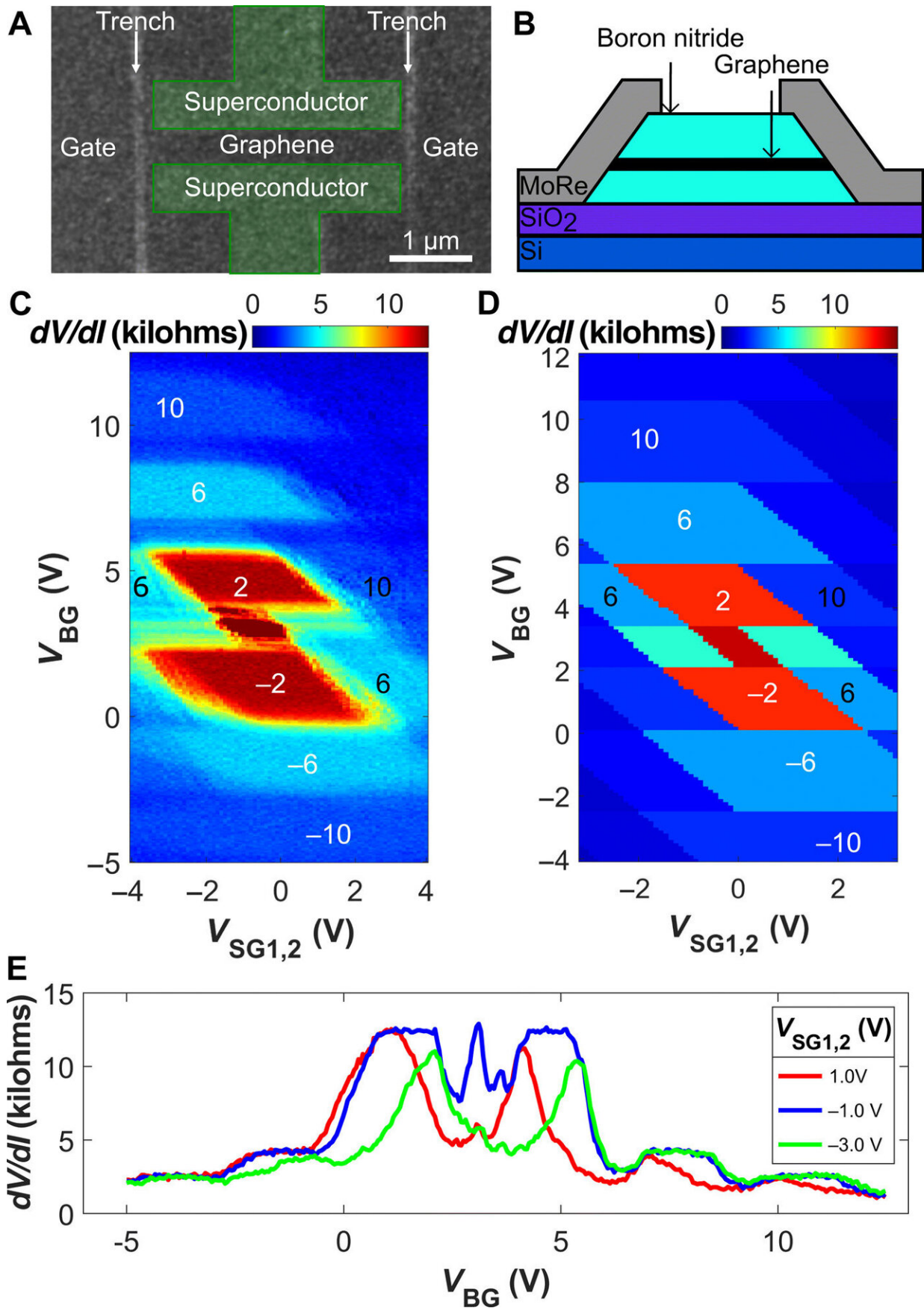
with a periodicity of ~ 0.6 mT. Panel (g) is similar to panel (d) but with only one side gate applied. This results in the supercurrent flowing only on one edge of the sample, as shown in panel (h). Panel (i) shows the magnetic interference pattern corresponding to panel (g). There is no variation in the pattern on this field scale, indicating a single, highly localized distribution of current. Credit: Science Advances, doi: 10.1126/sciadv.aaw8693

In a recent report published on *Science Advances*, Andrew Seredinski and co-workers presented a graphene-based Josephson junction with dedicated side gates fabricated from the same sheet of graphene as the junction itself. The interdisciplinary research team in the departments of physics, astronomy and advanced materials in the U.S. and Japan found the side gates to be highly efficient, allowing them to control carrier density along either edge of the junction across a wide range of magnetic fields. For example, they populated the next Landau level (where the number of electrons are directly proportional to the strength of the applied magnetic field) within magnetic fields in the 1 to 2-Tesla (T) range, to result in quantum Hall plateaus. Then when they introduced counter-propagating quantum Hall edge states along either side of the device, they observed a supercurrent localized along the edge of the junction. In the present work, they studied these supercurrents as a function of magnetic field and carrier density.

In quantum mechanics, physicists classify particles either as fermions or bosons. This classification is crucial to understand a variety of physical systems including lasers, metals and superconductors. Interactions between electrons or atoms in some two-dimensional (2-D) systems can lead to the formation of quasi particles that break from the fermion-boson dichotomy; to form 'non-Abelian' states of matter. Many experimental studies attempt to identify non-Abelian states in systems that manifest the quantum Hall (QH) effects (quantization of resistance

in two-dimensional electronic systems). The identification of such states will be useful for [quantum computation](#).

Physicists predict the interplay of spin-helical states and superconductivity to allow access to [non-Abelian](#) excitations such as [Majorana Zero modes](#) (MZM). These states may form the basis for quantum computing architectures, which take advantage of topological protections to [achieve fault tolerance](#) thus allowing a system to continue operating properly in the event of failure. Researchers aim to develop several techniques, including hybrid [superconductor-semiconducting](#) nanowires and superconductor-topological insulator structures for such quasiparticle-based applications. Recent research interest in [superconductivity](#) had also led to a [flurry of activity](#) at the interface of superconductivity and the quantum Hall (QH) effect. For instance, scientists have deduced that quasi-one-dimensional (1-D) superconducting contacts can [enable MZM and parafermions](#), while heterostructures of graphene and hexagonal boron nitride (BN) with [1-D superconducting contacts](#) can demonstrate remarkable contact transparency to observe [supercurrent in the QH regime](#). However, microscopic details of supercurrent in the QH regime hitherto [remain an open subject](#).

A

Trench   Trench

Gate   Superconductor   Gate

              Graphene

              Superconductor

                                1 µm

B

Boron nitride   Graphene

MoRe

SiO$_2$

Si

C

dV/dI (kilohms)

0   5   10

V_{BG} (V)

10

6

6   2   10

6

−2   6

−6

−10

$V_{SG1,2}$ (V)

−4   −2   0   2   4

D

dV/dI (kilohms)

0   5   10

V_{BG} (V)

12

10

8

6

10

6

6   2   10

−2   6

−6

−10

$V_{SG1,2}$ (V)

−2   0   2

E

dV/dI (kilohms)

15

10

5

0

$V_{SG1,2}$ (V)

1.0V
−1.0 V
−3.0 V

V_{BG} (V)

−5   0   5   10

Device layout and gate influence on QH plateaus. (A) Scanning electron microscopy (SEM) micrograph of the device prior to reactive ion etching. MoRe contacts are outlined and colored green for contrast. Two trenches (light gray), ~60 nm wide, separate the junction from the side gates. The MoRe contacts are spaced from the trenches by ~100-nm-wide regions of graphene, preventing direct contact between MoRe and the edge of the mesa. (B) Schematic side view of a vertical cross section of (A). (C) Resistance map as a function of back-gate voltage, VBG, and symmetrically applied side-gate voltages, VSG1 = VSG2, at B = 1.8 T. The diamond-shaped regions correspond to the plateaus of quantized resistance. Their horizontal boundaries (affected by VBG only) correspond to constant electron density in the bulk. The inclined side boundaries of the diamonds correspond to constant filling factors near the edges, where the influences of the back and the side gates compensate each other. The white numbers mark the sample's filling factor, while the black numbers at the high side gate mark sample conductance in units of e2/h. (D) Finite element electrostatic simulation of (C) reproducing the diamond-shaped regions of constant conductance. The conductance plateaus marked in (C) are marked similarly. (E) Sample resistance as a function of VBG at several VSG1,2, corresponding to vertical cross sections of (C). The curves show that the QH plateaus are best developed with the side gates set to −1 V. At VSG1,2 = − 3 V and +1 V, the plateaus shrink and become asymmetric between the electron and hole-doped sides, as is often found in samples without side gate control. Credit: Science Advances, doi: 10.1126/sciadv.aaw8693

In the present work, Seredinski et al. examined a graphene Josephson junction with two graphene side gates to directly manipulate QH edge states. They tuned each gate to change the Landau level filling factor along the edges to observe a supercurrent, solely localized along one edge. The team built the samples from graphene encapsulated in hexagonal boron nitride (BN) to protect devices from contamination and to yield ballistic transport across micrometre scales. They etched the

graphene-BN stack and then fabricated quasi-1-D contacts to the exposed region. They used molybdenum rhenium (MoRe), a type II superconductor and separated the 3-μm wide contacts by 500 nm to form the experimental setup. In the next step, they formed both the junction and side gates by etching narrow trenches on either side of the contacts, to efficiently control electron density along the edges of the junction—after applying voltage to the graphene regions. They did not overlap the etched trenches with the contacts and instead spaced them using a graphene strip, to prevent electrons from tunnelling directly from the superconductor to the edge.

When Seredinksi et al. applied a magnetic field perpendicular to the sample, the junction entered the QH (quantum Hall) regime. By 1.8 Tesla, the QH effect was very well developed and observed using resistance maps reproduced by a simple electrostatic simulation in the work. The research team gained more insight to the function of the device by applying the side gates independently. They observed the influence of the side gates on the conductances to show negligible cross-talk between the left gate on the right edge, and vice-versa. The scientists tuned the gates to induce a QH state to create counter-propagating states within the device. The team observed the QH supercurrent and its interference patterns as a region of suppressed resistance flanked by peaks; characteristic of a small supercurrent. The team regulated features of the device to localize the supercurrent to either junction.
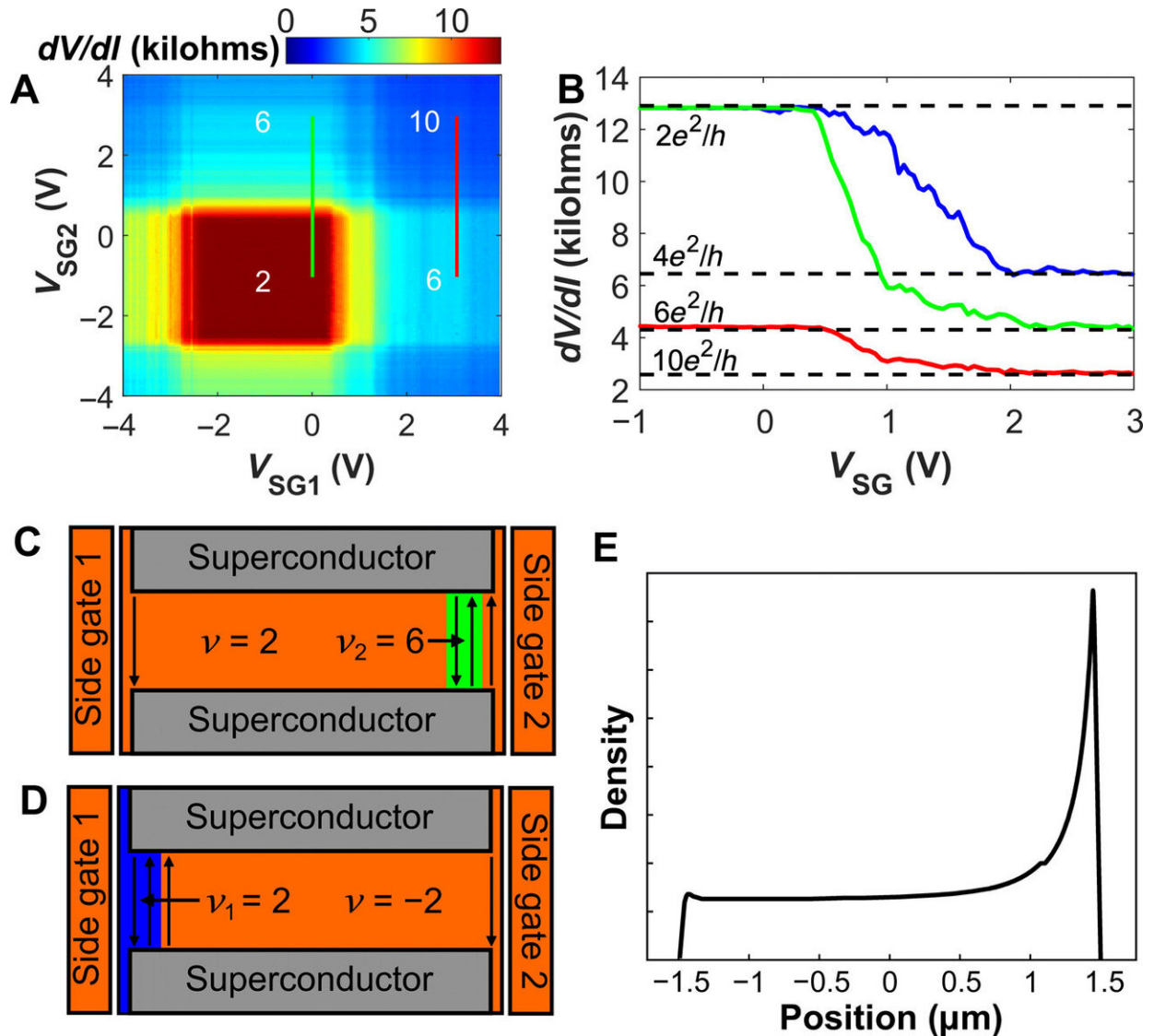
Side gate–induced QH plateaus. (A) dV/dI map plotted versus side-gate voltages V_{SG1} and V_{SG2} at B = 1.8 T. The back-gate voltage is fixed at V_{BG} = 4.7 V, corresponding to the bulk ν = 2 state. The numbers mark the sample conductance in units of e^2/h. (B) Sample resistance measured as a function of a single side gate. Green and red curves correspond to the vertical lines in (A) at V_{SG1} = 0 and 3 V, respectively (with V_{BG} = 4.7 V). The blue curve shows a similar trace with a bulk filling factor ν = − 2 (V_{BG} = 1.5 V), sweeping V_{SG1} with V_{SG2} = 0 V. (C and D) Schematics corresponding to the green and blue curves in (B) for V_{SG} greater than ~2 V. Additional edge channels are created near the gate, with local filling factor ν_2 = 6 (C, green region) and ν_1 = 2 (D, blue region). Additional conductance is equal to $4e^2/h$ and $2e^2/h$ in (C) and (D), respectively,

on top of the base conductance of 2e2/h, as is observed for the blue and green curves in (B). (E) Schematic of the carrier density within the graphene junction as a function of position when SG2 (1) is active (passive), akin to (C). Credit: Science Advances, doi: 10.1126/sciadv.aaw8693.

The supercurrent did not vary for small changes in the magnetic field. For example, when the team turned a side-gate on, the distance between the counter-propagating edge channels in the device facilitated the coupling of edge states to the superconductor—for the supercurrent to appear. When they applied both sides of the gates simultaneously, the dependence of the supercurrent on magnetic fields completely changed. The resulting map demonstrated a superconducting quantum interference device (SQUID)-like interference pattern. When Seredinski et al. explored the device as an interferometer for QH supercurrents, they changed the field to 1 T to observe a more robust supercharging signature. They obtained the pattern of resistance oscillations in the magnetic field, where the period of oscillations was independent of the gate voltage, while the phase of oscillations varied with the gate.
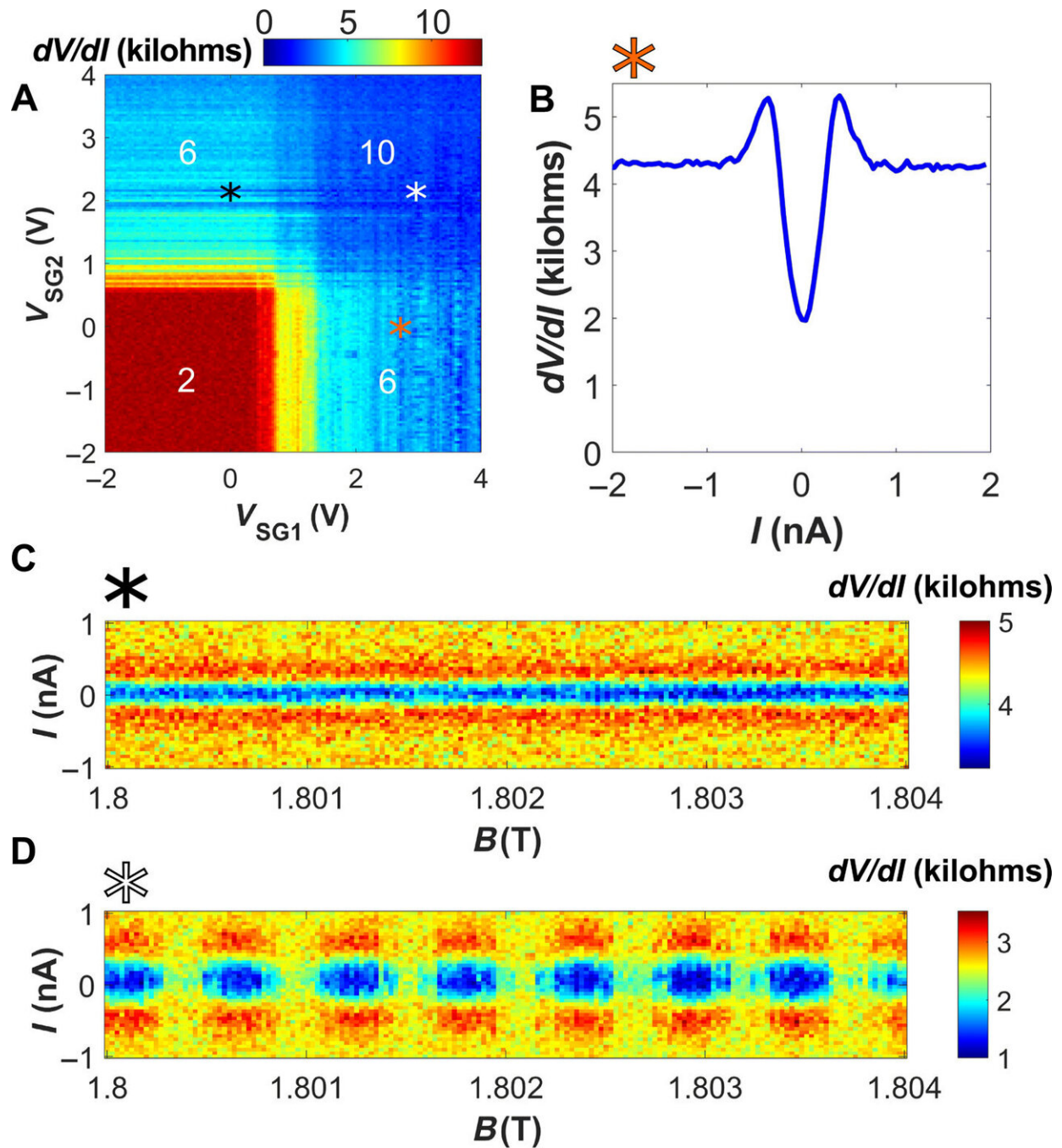
QH supercurrent and its interference patterns. (A) Differential resistance map versus VSG1,2 as in Fig. 2A but measured with 0 nA DC current bias, allowing observation of suppressed resistance due to the supercurrent. The gate voltage locations of (B) to (D) are marked by (B) an orange asterisk, (C) a black asterisk, and (D) a white asterisk. (B) dV/dI measured versus I, indicating the presence of a supercurrent on top of the quantized h/6e2 plateau. (C) Current-magnetic field

map of the differential resistance when a supercurrent is induced along one side of the sample only with VSG2, while VSG1 stays at zero. The supercurrent is not sensitive to an incremental change of field on a few millitesla scale. (D) A similar map with both side gates inducing supercurrent, showing a SQUID-like interference pattern. Credit: Science Advances, doi: 10.1126/sciadv.aaw8693.

In an additional interference pattern, the research team observed the difference in the sample resistance between 0 and 10 nanoampere (nA) DC bias, to highlight the superconducting regions. They measured the map as a function of both side gates and observed the interference corresponding to supercurrents flowing along the side gate-1 (SG1) and side gate-2 (SG2). The two gates presented comparable efficiency. When the scientists increased the voltage of one gate, they decreased the voltage of the opposing gate to roughly maintain the same area of the SQUID (superconducting quantum interference device). These area changes were sufficient to evolve the phase of difference across the junction, although too small to create noticeable changes in the magnetic field periodicity.

A *dV/dI* (kilohms)

C *dV/dI* (kilohms)

B

D ΔR (kilohms)
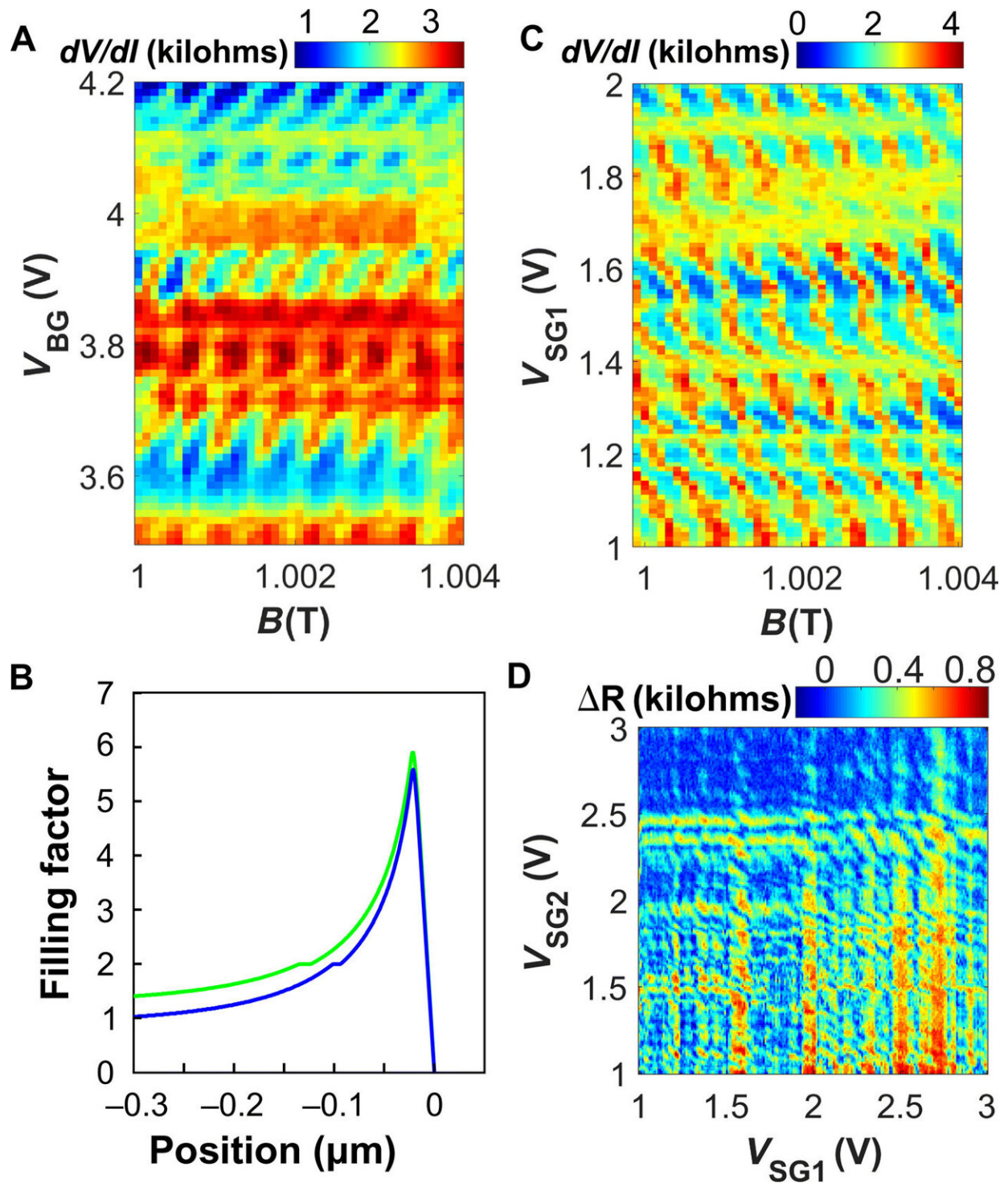
QH supercurrent interferometry. (A) dV/dI map measured at VSG1 = 2.34 V and VSG2 = 2.36 V as a function of VBG and B near 1 T. For a given gate voltage, the regions of suppressed resistance correspond to stronger supercurrent. The phase of the oscillations depends on the gate voltage, indicating that the

interference area decreases with the gate voltage (positive dVBG/dB). This is explained by the inner edge states moving further inward as the electron density grows [schematic in (B)]. (B) Schematic of carrier density in the sample along the midline between the contacts. The blue line represents some baseline charge density; the green line shows a higher back gate voltage. (C) dV/dI map similar to (A) measured as a function of B and SG1 voltage for VBG = 3.8 V. The map shows an interference pattern with a slope opposite that in (A), indicating that the interference area increases with gate voltage as the electrons are pushed further toward the gate. (D) ΔR map displaying the difference between the resistance in the 0 and 10 nA DC bias conditions, measured at 1 T with VBG = 3.9 V. Both side-gate voltages are high enough to induce a supercurrent (VSG1,2 > 1 V), and the vertical and horizontal features correspond to the supercurrent induced by SG1 or SG2, respectively. At their intersections, additional diagonal features appear, indicating interference between the supercurrents on the two sides of the sample. The fringes have a slope ~ −1, suggesting comparable efficiency of the two side gates. Credit: Science Advances, doi: 10.1126/sciadv.aaw8693.

In this way, Andrew Seredinski and colleagues showed native graphene side gates to be remarkably efficient in controlling edge state propagation in the quantum Hall (QH) regime. They observed supercurrents induced by the side gates, to be carried by the QH edge states. These supercurrents flowed independently on each edge of the device and could be controlled independently by their corresponding gates. The experiment opens a promising new route to couple superconductors with QH edge states to induce non-Abelian excitations to form the basis of quantum computing architectures.

  More information: Quantum Hall–based superconducting interference device. advances.sciencemag.org/content/5/9/eaaw8693 Andrew Seredinski et al. 13 September 2019, *Science Advances*.

Non-Abelian states of matter.

www.ncbi.nlm.nih.gov/pubmed/20220836/ Stern A. et al. March 2010, *Nature*.

Non-Abelian anyons and topological quantum computation. [journals.aps.org/rmp/abstract/ … 3/RevModPhys.80.1083](journals.aps.org/rmp/abstract/) Chetan Nayak et al. 12 Sept 2008, *Reviews of Modern Physics*, APS Journals.

Supercurrent in the quantum Hall regime science.sciencemag.org/content/352/6288/966 Amet F. et al. 20 May 2016, *Science*.